Naval Research Laboratory
Washington, DC 20375-5320

NRL/MR/6440--97-7994

Design and Simulation of a Partially Confined Detonation Facility

CHARLES A. LIND
JAY P. BORIS
ELAINE S. ORAN

Laboratory for Computational Physics and Fluid Dynamics

September 30, 1997

REPORT DOCUMENTATION PAGE

Form Approved
OMB No. 0704-0188

1. AGENCY USE ONLY (*Leave Blank*)	2. REPORT DATE	3. REPORT TYPE AND DATES COVERED
	September 30, 1997	

4. TITLE AND SUBTITLE

Design and Simulation of a Partially Confined Detonation Facility

5. FUNDING NUMBERS

6. AUTHOR(S)

Charles A. Lind, Jay P. Boris, and Elaine S. Oran

7. PERFORMING ORGANIZATION NAME(S) AND ADDRESS(ES)

Naval Research Laboratory
Washington, DC 20375-5320

8. PERFORMING ORGANIZATION REPORT NUMBER

NRL/MR/6440--97-7994

9. SPONSORING/MONITORING AGENCY NAME(S) AND ADDRESS(ES)

10. SPONSORING/MONITORING AGENCY REPORT NUMBER

11. SUPPLEMENTARY NOTES

12a. DISTRIBUTION/AVAILABILITY STATEMENT

Approved for public release; distribution unlimited.

12b. DISTRIBUTION CODE

13. ABSTRACT (*Maximum 200 words*)

It is estimated that more than 500,000 tons of obsolete and unwanted conventional weapons exists in the United States. The disposal of these unexploded ordnances, in an environmentally sound and cost effective way, is of tantamount importance. Open-air burning and open-air detonation (OB/OD) are two of the most widely used methods to dispose of these unwanted energetic materials. This report describes our efforts to improve the environmental safety of OB/OD operations through the design and testing of a new, large-scale, partially confined facility that minimizes the adverse affects of far field noise and maximizes the afterburn of explosive byproducts. Several designs were evaluated by a series of axisymmetric, time-dependent numerical simulations using FAST3D, a Flux-Corrected Transport based code optimized for parallel processing. The simulations are used to investigate various facility geometries and shapes and charge size, shape, and placement to determine combinations that result in acceptable detonations. Results from the simulations were used to determine the structural response of the facility to the initial blast.

14. SUBJECT TERMS

Open air detonation
OD/OB
FAST3D
Flux-corrected transport
3D flow simulation
Continuity equations
Fluid dynamics

15. NUMBER OF PAGES

26

16. PRICE CODE

17. SECURITY CLASSIFICATION OF REPORT	18. SECURITY CLASSIFICATION OF THIS PAGE	19. SECURITY CLASSIFICATION OF ABSTRACT	20. LIMITATION OF ABSTRACT
UNCLASSIFIED	UNCLASSIFIED	UNCLASSIFIED	UL

CONTENTS

Design and Simulation of a Partially Confined Detonation Facility

1. INTRODUCTION

Stockpiles of conventional munitions, propellants, and related materials have accumulated in hundreds of depots in the United States and abroad. In the United States alone, this inventory is estimated to be in excess of 500,000 tons, accumulating at a rate of 40,000 to 50,000 tons per year and covering more than 11 million acres of land. The worldwide demilitarization (demil) inventory estimate is on the order of 9 million tons. Base realignment and closure is slated for many of the arsenals and depots, increasing the urgency for finding safe, inexpensive, and environmentally acceptable methods to dispose of the demil inventory.[1]

A traditional method for disposal of unwanted inventory has been through unregulated open burn (OB) or open detonation (OD) in open pits. However, noise, safety, and environmental concerns have brought these activities largely to a halt, stimulating a search for alternative disposal techniques. A number of new techniques are now in use. Some of the inventory can be synthesized into reusable materials or can be rendered harmless using exotic chemical or biological processes. However, these alternative disposal technologies do not address the full magnitude and scope of the demil problem, and they entail significant additional expense and pose potential environmental impacts in the form of processing byproducts. Also, some of the inventory has become too unstable and dangerous to handle or move to processing facilities. Thus, cost and safety issues force the demil community to reexamine the possibility of using large-scale OB/OD, with appropriate controls and mitigation, as a means to eliminate the bulk of the demil inventory.

Currently, there are three primary methods for disposing of this large inventory: incineration; disassembly, recovery, and recycling (DRC); and open air burning and detonation (OB/OD). The environmentally preferred methods of disposal are incineration or DRC. However, these methods cannot be used presently since the product composition of most of this inventory is either unknown, unstable, obsolete, or degraded. In addition, due to the size of the current inventory, disassembly of

Manuscript approved August 27, 1997.

the munitions cannot be justified. Hence, for the materials in question, OB/OD is the only feasible disposal technique currently available.[2,3]

Although a few small-scale demilitarization operations are presently permitted, large scale OB/OD operations have ceased due to a lack of documentation certifying the safety and efficacy of this inventory disposal technique. The Naval Research Laboratory (NRL), along with the Dugway Proving Ground (DPG) and the Office of Research and Development of the U.S. Environmental Protection Agency (EPA) are cooperating in a study sponsored by the Department of Defense Strategic Environmental Research and Development Program (SERDP) designed to address these concerns and to define the noise mitigation and safety constraints under which large scale OB/OD activities can be conducted in an environmentally safe manner. The key component of the work presented here is the documentation of partially confined OB/OD detonations and its impact on the facility and the environment. The goal of SERDP is to devise, test, and implement procedures that will meet the Nation's demil inventory disposal needs in a cost-effective, safe, and environmentally responsible manner.

This report presents numerical calculations that characterize the explosion sources in an axisymmetric, partially confined, detonation containment facility, which we call the ODOBi. The calculations are performed with the computational fluids dynamics (CFD) model FAST3D[4], which combines a time-dependent, three–dimensional convective flow solver with a technique for resolving geometrically complex flow domains. The simulations provide detailed information on the flow patterns and variation and distribution of the thermodynamic properties throughout the facility. An approximation to the time dependent displacement of the structures walls is modeled as a harmonic oscillator with forcing and damping terms. Results of this analysis gives an estimate of the tension in the walls and hence the survivability of the facility. This work also details the complex fluid-structure interaction. The goal of the simulations was to test various geometric configurations, charge shapes, charge placement and charge size and to determine which combination resulted in the most efficient detonation and least environmental impact. Results of the present work assisted in the design of the full scale ODOBi, located at Dugway Proving Ground.[5,6]

2. NUMERICAL MODEL

The numerical model solves the time-dependent conservation equations for mass, momentum, and total energy:

$$\frac{\partial \rho}{\partial t} = -\nabla \cdot (\rho V) \tag{1a}$$

$$\frac{\partial (\rho V)}{\partial t} = -\nabla \cdot (\rho V V) - \nabla P \tag{1b}$$

$$\frac{\partial E}{\partial t} = -\nabla \cdot (EV) - \nabla \cdot (PV) \tag{1c}$$

where ρ is the fluid density, t is time, V is the fluid velocity, P is pressure, and E is the fluid energy density. This set of equations is closed by including the perfect gas equation of state in the definition of the total energy

$$E = \frac{P}{\gamma - 1} + \frac{V^2}{2}. \tag{1d}$$

Given a set of initial and boundary conditions, Equations (1) are solved using FAST3D, a three–dimensional flow solver that combines the Flux-Corrected Transport (FCT) algorithm with the Virtual Cell Embedding (VCE) method for solving geometrically complex configurations.

Flux-Corrected Transport [7,8] is a high-order, monotone, positivity-preserving algorithm for solving generalized continuity equations with source terms. Monotonicity is achieved by introducing a diffusive flux and later correcting the calculated results with an antidiffusive flux modified by a flux limiter. Operator splitting techniques are used to divide the solution into a series of one-dimensional integrations along each coordinate direction.

Virtual Cell Embedding (VCE) is a method for representing and computing the flow around bodies of arbitrary shape on a Cartesian grid.[9–11] It does this without sacrificing computational speed or memory. Although the grid remains orthogonal, the VCE method effectively increases the number of mesh points in the vicinity of complex geometric shapes, thus eliminating the "staircase" effects. If any cell is partially obstructed by an obstacle or wall, the flux calculation is modified by subdividing each of the partially blocked cells into a number of smaller subcells from which the areas and volumes may be computed to arbitrary accuracy. Only those cells next to the boundary are refined or subdivided. The term "virtual" means that the subcells embedded within each computational cell are not stored in memory, but are stored in a list at the location indicated by a pointer stored in the parent cell. Hence, during the integration of the fluid equations, the correct areas and volumes are used for the cells bordering the body.

In addition to using these more accurate face areas and volumes, a flux coupling vector between the integration directions is calculated in boundary cells. This flux coupling vector is used in the direction-split integration of the flow solution to correct the apparent fluid compression in each cell caused by the body obstructing a cell. The flux coupling term is computed and used as a source term in the FCT integration.

2.1 Physical Model and Initial Conditions

Figure 1a shows a schematic of the computational domain in a regime that consists of the facility containing an explosive charge and the surrounding region. The flowfield is assumed symmetric about the centerline. As the computational grid size affects the accuracy of the solution, several different grid resolutions were used in this work and are summarized in Table 1. The grid was stretched in regions far from the facility, so that the last 40 computational cells in each direction are geometrically stretched. These stretched cells represent the part of the region in open space. This stretching results in the physical extents of the computational domain shown in the last column of Table 1 of Section 3.

A first–order extrapolation is used for the outflow conditions on the right and upper boundaries; a solid wall condition is set for the bottom boundary; and a symmetric boundary condition is used for the centerline.

The computational domain is extended far enough in the r and z directions to assure that the boundaries do not influence the complex flow structure associated with the interaction of the detonation with the facility. The figures presented in this paper, however, only show the part of the computational domain which includes the facility and the region immediately surrounding the facility.

It is assumed that the initial RDX charge has a material density of 1 g/cm^3 and an energetic yield of 2 $\times 10^{10}$ ergs/g. It is further assumed that the increased pressure and density associated with this charge is uniformally distributed across 40 computational cells and that the energy release is instantaneous. The remainder of the flowfield is initially set to ambient conditions. Emphasis is placed on the global effects of the shock interactions associated with a high energy blast, hence the physics of chemical reactions has not modeled.

2.2 Structural Loading Model

The pressure distribution along the inside wall is used as the source term to a driven oscillator which is then integrated to give an approximation to the radial response, and hence tension, of the wall. This calculation is done independently of the flowfield calculation. This model gives a conservative approximation to the time-dependent displacement of the shell. The equation used for modeling the displacement of the cylindrical walls as a function of time, taking into account damping, restoring, and driven forces[12] is

$$m\frac{d^2\xi}{dt^2} = -\alpha\frac{d\xi}{dt} - k\xi + F_o(t). \tag{2a}$$

In this equation m is the mass, ξ is the radial displacement of the walls, α is the damping factor, k is the spring constant, and F_o is the internal force on the wall due to the time dependent pressure, $P(t)$.

The mass, m, may be written as

$$m = \rho_w h A, \tag{2b}$$

where ρ_w is the density of the wall, h is the thickness, and A is the area. In addition, the ratio k/m, which is equal to the square of the frequency, ω, may be written in terms of the material properties of the wall. For the cylindrical portion of the facility,

$$\left(\frac{k}{m}\right)_c = \omega_c^2 = \frac{2E}{(2-\nu)\rho_w R^2}\ , \tag{2c}$$

where E is Young's modulus, ν is Poisson's ratio, and R is the radius of the cylinder. For the spherical endcaps, the ratio k/m is

$$\left(\frac{k}{m}\right)_s = \omega_s^2 = \frac{2E}{(1-\nu)\rho_w R^2}\ . \tag{2d}$$

Combining Equations 2a– 2d, the following second–order differential equation is obtained

$$\frac{d^2\xi}{dt^2} = -\alpha\frac{d\xi}{dt} - \omega_{c,s}^2\xi + \frac{P(t)}{\rho h}\ . \tag{2e}$$

This equation is then integrated to obtain the velocity and displacement of the wall as a function of time. The tension in the walls as a function of time, $T(t)$, is then obtained from the relationship

$$T(t) = \frac{kR\xi(t)}{h}\ . \tag{2f}$$

For this work the wall is assumed to be steel, which has the following material properties:

- Young's modulus: $E = 2.1 \times 10^{12}$ dynes/cm^2
- Poisson's ratio: $\nu = 0.3$
- Density: $\rho_w = 8.0\ gm/cm^3$

3. RESULTS AND DISCUSSION

Run #	RDX (lbs)	Height (cm)	$\Delta r, z$ (cm)	Grid Size	Wall (cm)	Exit (cm)	Physical Dimensions (cm)
R1	50	100	2	192×448	2.54	50	843×1580
R2	50	182	2	192×384	2.54	50	843×1350
R3	50	265	2	192×384	2.54	50	843×1350
R4	50	182	2	192×448	2.54	76	843×1350
R5	50	182	1	320×768	2.54	76	698×1360
R6	50	265	2	192×448	5.08	76	843×1580
R7	100	182	2	192×448	5.08	76	843×1580

Table 1: Summary of Simulations.

In this work, the pressure loading on the interior walls of the ODOBi and the complex shock interactions within the facility were studied. The pressure loading analysis helped define the integrity of the facility and the shock interaction analysis assisted in understanding the global features of the complex shock interactions and in determining ways to maximize the burning of the byproducts.

3.1 Variation of Size of Exit Opening

3.1.1 Small (1 m) Opening, 50 lb Charge

The first three simulations, Runs 1 - 3, described in Table 1, were performed on a facility with an opening of 1 meter (m) in diameter, as shown in Figure 2a. The simulations modeled the explosion of 50 lbs of RDX spherically distributed along the centerline at 1 m, 1.82 m, and 2.65 m locations, respectively. The positions correspond to locations near the bottom of the lower hemispherical shell, near the top of the bottom hemispherical shell, and near the center of the ODOBi, respectively.

Figures 4 - 5 display two dimensional snapshots of the density field at selected times for Run 2, described above. After 1 ms, the initially spherical blast begins to impinge on the lower end cap, resulting in uniformly high pressure along this lower surface, reaching a maximum pressure of 96 atm. After reflecting from this lower surface the shock is refocussed. The upper part of the expanding initial shock continues to propagate upward until it interacts with the upper end cap. A short time later this upward moving shock impinges on the upper end cap and, due to

its constricted opening, is also refocussed and subsequently moves downward. Shortly after 3 ms the high velocity flow begins to exit the chamber. The remaining plots show the numerous, and complex, shock interactions and reflections, as well as the development of the exiting plume.

Pressure distributions along the inside wall of the facility, from the bottom of the lower cap through the top opening, as a function of time, are presented in Figures 6 - 8. In these plots the x–axis represents the distance as measured along the inner surface of the wall, from the bottom of the ODOBi through the top opening. Figure 3 shows the relationship between the wall location and the distance along the wall for the small opening ODOBi (Figure 3a) and the large opening ODOBi (Figure 3b).

Figures 6 - 8 show that the highest computed pressure load, 210 atm., on the interior wall of the ODOBi occurs when the charge is placed at a height of 1 m, followed by 2.65 m with 182 atm. and 1.82 m with 96 atm.

Results for the 1 m height location, shown in Figure 6, indicate that the peak pressure occurs at the floor within 0.5 ms of the initial blast. A secondary peak occurs almost 4 ms later near the inside top shoulder of the ODOBi. The reflected shock causes a tertiary peak in the pressure to occur at approximately 7.5 ms after the initial blast.

Figure 7 shows the results for Run 2 (charge 1.82 m above floor). This higher placement of the charge results in an almost uniform pressure load on the lower hemispherical cap. As in the previous case, there are three dominate local peak pressures. The first occurring within the uniform loading region on the lower cap, peaking at 96 atm. The second local maximum again occurs after 3.5 ms at the inside top shoulder, as the spherically expanding blast strikes the chamber wall just inside the junction of the cylinder and the hemispherical end cap peaking at 65 atm. The third local maximum occurs 9.6 ms later and is located at the bottom of the lower end cap. This high pressure results from the reflection of the blast off the top of the constricted opening and subsequent refocusing at the bottom, as shown in Figures 4 - 5.

Figure 8 shows the pressure as a function of time when the charge is placed 2.65 m above the floor. Notice that after 1 ms there is a peak in the pressure loading on the side wall due to the expansion of the initial blast. However, the greatest pressure loading occurs at 182 atm., after the shock has reflected off the side wall and onto the floor, 3 ms after the initial blast.

Figures 9 - 11 show the results of the tension analysis as a function of time for Runs 1 - 3. The tension calculation assumed a 2.54 cm thick wall. These figures show the wall oscillations and how the phase of these oscillations varies along the inside wall depending on the location of the initial blast. For Run 1, the maximum tension observed was 132,400 PSI and the minimum (a compression) was 95,100 PSI. This maximum, located at 600 cm along the walls between 5.0 - 5.5 ms, resulted from the upward moving shock being focused due to the constricting area. When the charge is placed at 1.82 m, the maximum tension is 63,900 PSI and the maximum compression is 50,800 PSI, as shown in Figure 10. Raising the charge to a height of 2.65 m increases the maximum tension and compression in the cylindrical part of the facility to 79,700 PSI and 65,700 PSI, respectively, as shown in Figure 11.

For the steel being considered in this work, the maximum allowable tension is 70,000 PSI. This means that of the three charge locations investigated, the integrity of the ODOBi is assured only when the 50 lb. charge is placed at a height of 1.82 m.

If damping is added to the ODOBi walls, for example, by placing a berm around the ODOBi, it would be possible to decrease the maximum tension of the walls. As an example, by adding only 5% damping to the walls and repeating the tensile analysis for Run 3, as shown in Figure 12, the maximum tension decreases to 62,800 PSI. This represents a 21% decrease in the maximum tension when compared with no damping and the same charge height, as shown in Figure 11.

3.1.2 Large (1.5 m) Opening, 50 lb Charge

The exit opening was increased to 1.5 m, in order to determine the effects of a less flow constricting exit. For this case, a 50 lb RDX charge is placed at 1.82 m above the bottom of the ODOBi floor. This location was selected since, of the three heights simulated, this particular height resulted in the smallest loading. Figure 13 shows the pressure over the interior walls of the ODOBi for times less than 10 ms.

Figure 14 shows the pressure over the interior walls of the ODOBi between 10 and 20 ms after the blast. The trends are similar to those for the 1 m opening, Run 2. In particular, there are two notable pressure peaks occurring at two different times in the run. The first peak (96.9 atm.) occurs after 1.0 ms, when the expanding blast strikes the chamber wall just inside the junction of the cylinder and the lower hemispherical end cap. At this location the shock transitions from

direct to Mach reflection, and the end cap is focusing the blast so the pressure is actually somewhat higher than it is directly below the initial charge. The second local pressure maximum occurs very near the bottom of the lower end cap at 9.7 ms. This local maximum pressure (55.4 atm.) occurs because the shock is reflected off the top of the chamber and is subsequently refocussed.

This shock refocusing is again shown in Figure 15, which is the time history of the pressure along the centerline of the ODOBi, as measured from the base of the facility through the top opening. This figure shows the initial spherical blast traveling symmetrically upward and downward (right and left, respectively, in the figure) and having an initial peak pressure of 670 atm. At about 1 ms the shock reflects off the lower endcap (z = 4 cm). At 2 ms the shock rebounding from the lower end cap and the side walls reaches the vicinity of the initial explosion and the pressure increases to 92 atm. A short time later, 2.3 ms after the initial blast, there is another localized region of high pressure (147 atm.) along the centerline axis. At this point, the initial blast is just below the upper end cap, 3.5 m above the floor, the high pressure results from the shock being refocussed. At 5.7 ms after the initial detonation, another localized peak pressure of 139 atm. occurs 2.3 m above the floor and results from the original shock being refocussed shock.

The tension in the steel along the inner walls of the ODOBi for Run 4 is shown in Figure 16. This figure indicates that the maximum tension is 60,100 PSI and is located 1.2 m along the inner walls after 1.7 ms. This time corresponds to the period just after the initial shock has reached this location. Compared with the 1 m opening case, Run 2, the larger opening results in a 6% decrease in the maximum tension.

3.2 Grid–Resolution Study

In the unstretched region, the spacing of the grid was reduced by 50%, from 2 cm to 1 cm, to determine the effect of grid spacing on the calculated results. Figure 17 shows the pressure distribution as a function of time over the interior walls of the ODOBi for this simulation, Run 5, which has the same physical parameters as Run 4. Comparison of Figure 17 (Run 5) to Figure 13 (Run 4) indicates that the predicted pressures are similar. Specifically, the maximum peak pressure is overestimated by 14% when using the coarser grid. Also, a comparison of the tension analysis of Run 5 (Figure 18) to that of Run 4 (Figure 16) shows that the fine–grid maximum tension is 56,400 PSI, as compared to the coarser–grid value of 60,100 PSI, a difference of 6%. Thus it appears that the 2 cm resolution calculation will provide a conservative estimate to the loads on

the structure.

3.3 Cylindrically Shaped Charge

3.3.1 Large (1.5 m) Opening, 50 lb Charge

In order to try to minimize the pressure loading on the ODOBi, as well as to better model the types of munitions which would most likely be used in such a facility, the detonation of an elongated 50 lbs charge of RDX was simulated. This case is denoted as Run 6. The charge, which was 122 cm in length and 26 cm in radius, is centered at 2.65 m, as shown in Figure 2b. Figure 19 shows the pressure over the interior wall of the ODOBi for times up to 10 ms. A comparison between the cylindrically shaped charge and the similar simulation for the spherically shaped charge, shown in Figure 8, shows that the peak pressure on the wall is approximately 2.5 times greater for the cylindrically shaped charge than for the spherically shaped charge. This result is not surprising, since most of the charge distribution for the cylindrical charge is parallel to the wall. In order to accommodate this higher pressure, the wall thickness was increased to 5.08 cm and 5% damping was added in the tension model. The results from the tension analysis are shown in Figure 20. The result is that the nearly symmetric ringing in the chamber is decreased.

3.3.2 Large (1.5 m) Opening, 100 lb Charge

The size of the cylindrically shaped charge was doubled to 100 lbs and placed 1.82 m above the floor for this simulation, Run 7. This charge has the same physical dimensions as the charge in Run 6, but the initial density and pressure were proportionally increased. Figure 21 shows the pressure over the interior walls of the ODOBi for times less that 10 ms. Although the pressure resulting from the initial blast is distributed over a much larger region for times less than 1 ms, as compared to Figure 19 of Run 6, the peak pressure is more the 2.5 times higher. In addition to the initial peak pressure, there are two other times at which the peak pressure on the bottom of the ODOBi reaches very high values: 3 ms and 9 ms For these times, the peak pressure is 186 atm. and 496 atm., respectively, and are due to the multiple reflections of the shocks inside the facility. The results from the tension analysis are shown in Figure 22. For this tension analysis no damping was used, but a correction was made for the end caps being spherically shaped. The periodicity of the oscillation is clearly evident in this figure, which has a peak tension of 106,300 PSI.

4. CONCLUSIONS

This work represents a study of a prototype partially confined detonation facility, the ODOBi, which has been now been constructed at the Dugway Proving Ground. The simulations were performed using FAST3D, a multi–dimensional, time dependent, flux-corrected transport based code. Both the pressure loading on the interior walls of the facility as well as the complex shock interactions within the facility were analyzed. Grid resolution, grid size, charge size, charge shape and charge placement were parametrically studied.

The results indicate that the charge should be placed below the center of the facility, otherwise the pressure loadings on the upper joint, just below upper hemispherical end cap and on the sides of the facility may adversely affect the structures integrity. Specifically, the computations suggest that the optimum location for the charge is between 1.7 and 2.0 meters above the bottom of the lower hemispherical cap. Detonation of charges up to 50 lb should be safe in the ODOBi, although some damping of the walls may be required for the larger charges.

The simulations include initial energy release due to the detonation, but do include subsequent chemical reactions. As our model development effort continues, appropriate chemical reaction, heat release, thermal conduction, and molecular diffusion models will be incorporated into this axisymmetric flow model. In the reactive flow simulations, we would expect that the reactive dynamics and afterburn of the material as it mixes with air will have some effect on the flow patterns within the facility, and may change the pressure loading on the facility.

The symmetry of the present ODOBi resulted in spatially and temporally localized high pressure regions. Future studies will address how breaking the symmetry, by considering three–dimensional configurations, could lower the peak pressure and pressure loading on the walls.

5. ACKNOWLEDGMENTS

The authors would like to acknowledge R. J. Black, Alan P. Ohrt, and Chris A. Biltoft for their input and comments regarding this work. The authors would also like to thank Theodore R. Young and Alexandra M. Landsberg for their considerable assistance in implementing the parallel version of FAST3D. This work was sponsored by the Dugway Proving Ground, the Environmental Protection Agency and the Strategic Environmental Research and Development Program.

6. REFERENCES

1. Arbuckle, J. W., "Conventional Ammunition Demilitarization Program," in *4th Global Demil Symposium*, (Sparks NV), pp. 13–21, May 1996.
2. Biltoft, C. A., Oran, E. S., Boris, J., Lind, C. A., and Mitchell, W. J., "Source Characterization Modeling For Demil Operations," in *Proceedings of the 20th Army Science Conference*, (Salt Lake City, UT), pp. 219–220, June 1996.
3. Mitchell, W. J., Casey, J. L., Oran, E. S., Boris, J., Lind, C. A., Ohrt, A. P., and Watt, J., "Test Facility for Improving the Destruction Efficiency of OB and OD Technology," in *Proceedings of the 4th Global Demil Symposium*, (Sparks NV), pp. 400–410, May 1996.
4. Young, Jr., T. R., Landsberg, A. M., and Boris, J. P., "Implementation of the Full 3D FAST3D (FCT) Code Including Complex Geometry on the Intel iPSC/860 Parallel Computer," in *Proceedings of the 1993 Simulation Multiconference on the High Performance Computing Symposium*, (Arlington, VA), The Society for Computer Simulation, 1993.
5. Lind, C. A., Boris, J. P., Oran, E. S., Mitchell, W. J., and Wilcox, J. L., "The Response of an Open Air Detonation Facility to Blast Loading," in *Proceedings of the 1997 Structures Under Extreme Loading Conditions Symposium, PVP-Vol. 351* (Shin, Y. S., ed.), (Orlando, FL), pp. 109–125, ASME, July 27-31, 1997.
6. Lind, C. A., Boris, J. P., Oran, E. S., , Mitchell, W. J., and Black, R. J., "FAST3D Characterization of ODOBi, a Partially Confined Detonation Facility," in *Proceedings of the 1997 Global Demilitarization Symposium and Exhibition*, (Reno, NV), May 5-9, 1997.
7. Boris, J. P. and Book, D. L., "Flux-Corrected Transport 1. SHASTA, A Fluid Transport Algorithm That Works," *Journal of Computational Physics*, Vol. 11, 1973, pp. 38–69.
8. Boris, J. P., Landsberg, A. M., Oran, E. S., and Gardner, J. H., "LCPFCT – A Flux–Corrected Transport Algorithm for Solving Generalized Continuity Equations," NRL Memorandum Report 93-7192, 1993.
9. Landsberg, A. M., Boris, J. P., Young, Jr., T. R., and Scott, R. J., "Computing Complex Shocked Flows Through the Euler Equations," in *Proceedings of the 19th International Symposium on Shock Waves*, (Marseilles, France), 1993.
10. Landsberg, A. M., Young, Jr., T. R., and and, J. P. B., "An Efficient, Parallel Method for Solving Flows in Complex Three–Dimensional Geometries," *AIAA 94-0413*, January 1994.
11. Li, C., Kailasanath, K., and Oran, E. S., "Detonation Structures Generated by Multiple Shocks on Ram–Accelerator Projectiles," *Combustion and Flame*, Vol. 108, 1997, pp. 173–186.
12. Blake, A., *Practical Stress Analysis in Engineering Design.* New York: Dekker, Inc., 1982.

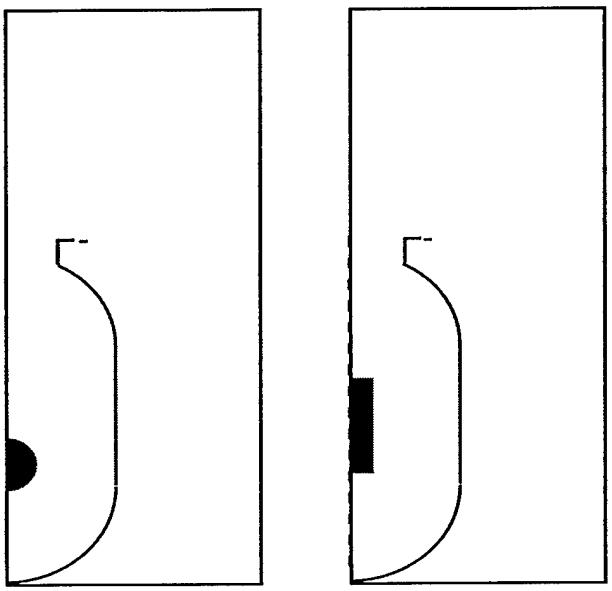

(a) Spherical (b) Cylindrical

Fig. 1: Schematic showing relative size and shape of the charges used in this work.

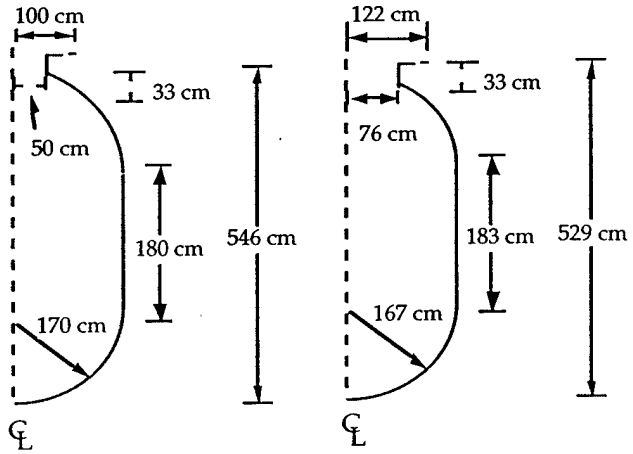

(a) Small Opening (b) Large Opening

Fig. 2: Schematic comparing the dimensions of the two facilities used in this work.

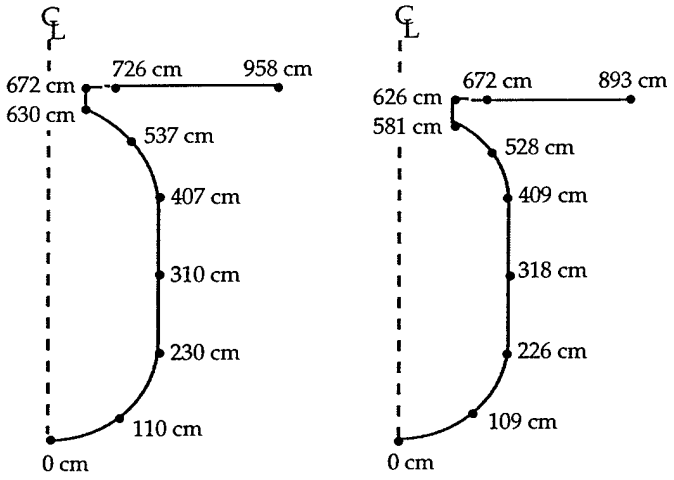

(a) Small Opening **(b) Large Opening**

Fig. 3: Schematic showing locations of various points along the inner surface of ODOBi.

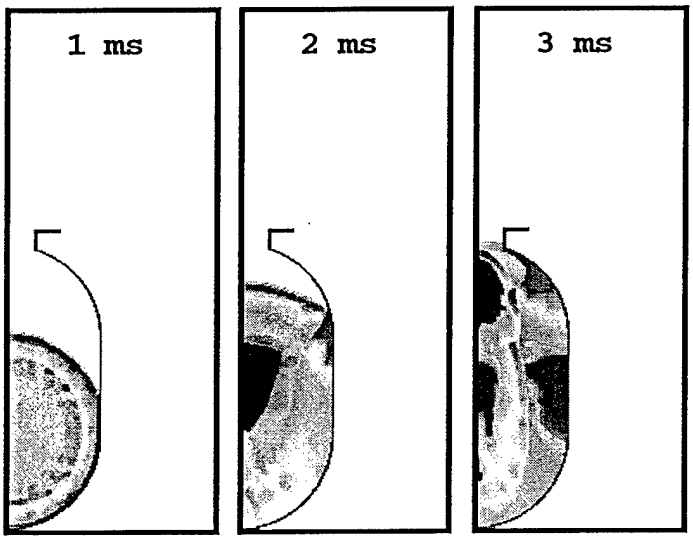

Fig. 4: Density contours for Run 2 at various times. (2.54 cm. walls, 2 cm. grid spacing, 1.82 m. height of detonation, 50 lbs. RDX and 1 m opening.)

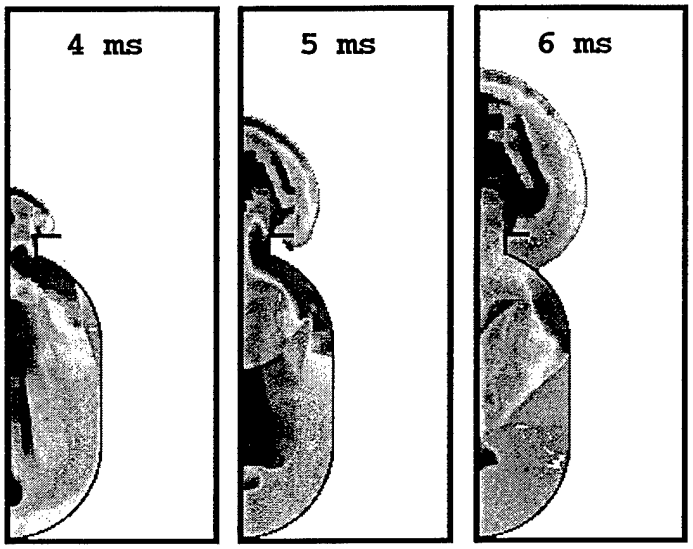

Fig. 5: Density contours for Run 2 at various times. (2.54 cm. walls, 2 cm. grid spacing, 1.82 m. height of detonation, 50 lbs. RDX and 1 m opening.)

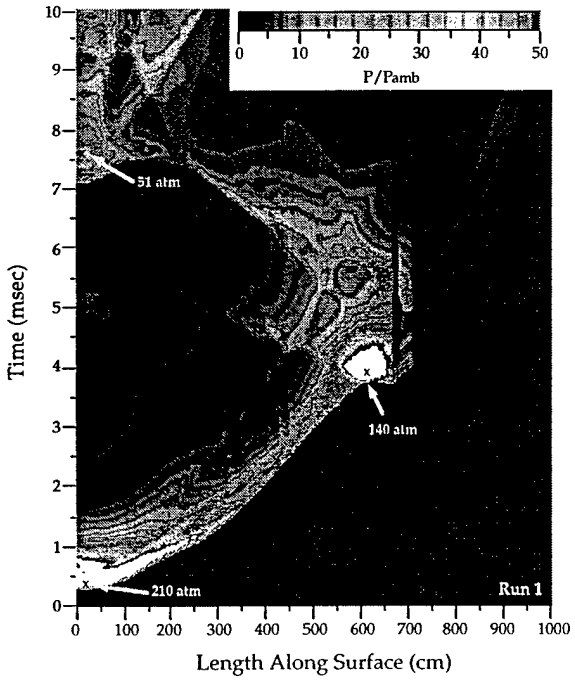

Fig. 6: Pressure as a function of time and wall location for Run 1. (2.54 cm. walls, 2 cm. grid spacing, 1 m. height of detonation, 50 lbs. RDX and 1 m opening.)

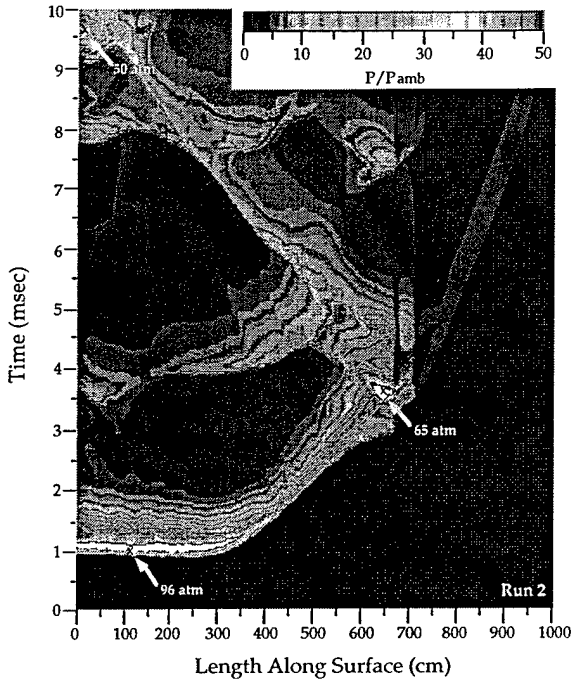

Fig. 7: Pressure as a function of time and wall location for Run 2. (2.54 cm. walls, 2 cm. grid spacing, 1.82 m. height of detonation, 50 lbs. RDX and 1 m opening.)

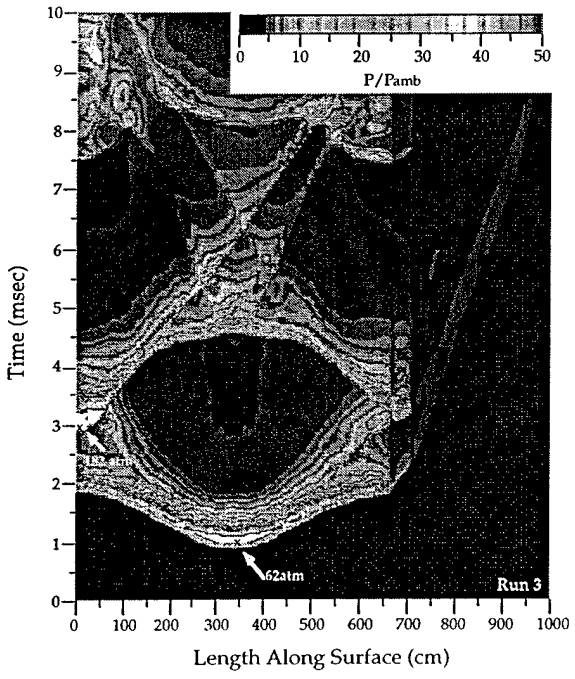

Fig. 8: Pressure as a function of time and wall location for Run 3. (2.54 cm. walls, 2 cm. grid spacing, 2.65 m. height of detonation, 50 lbs. RDX and 1 m opening.)

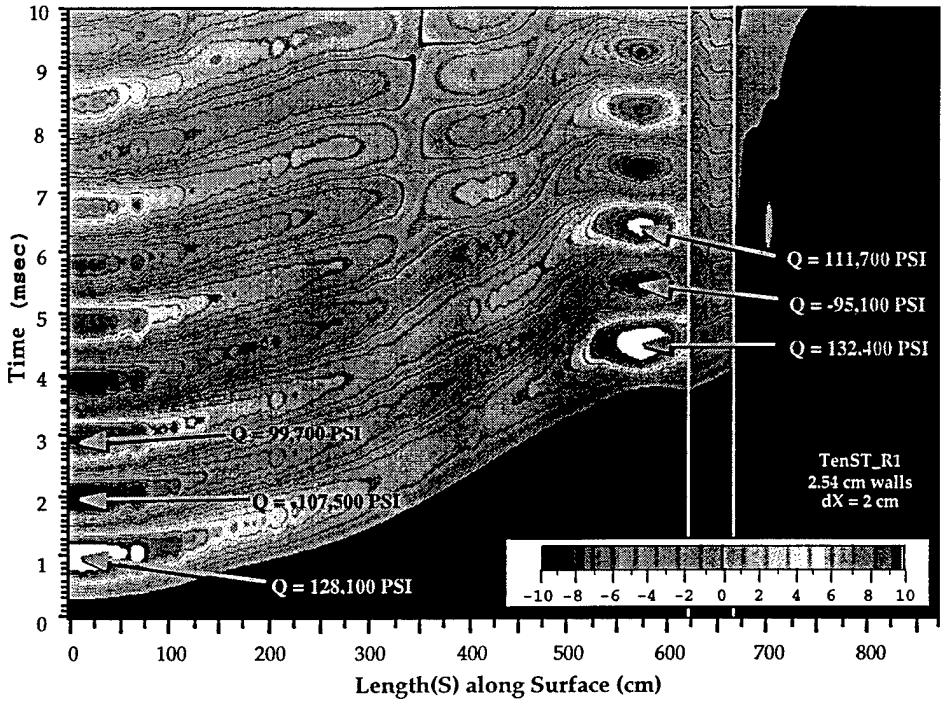

Fig. 9: Tension in the wall as a function of time and wall location for Run 1.

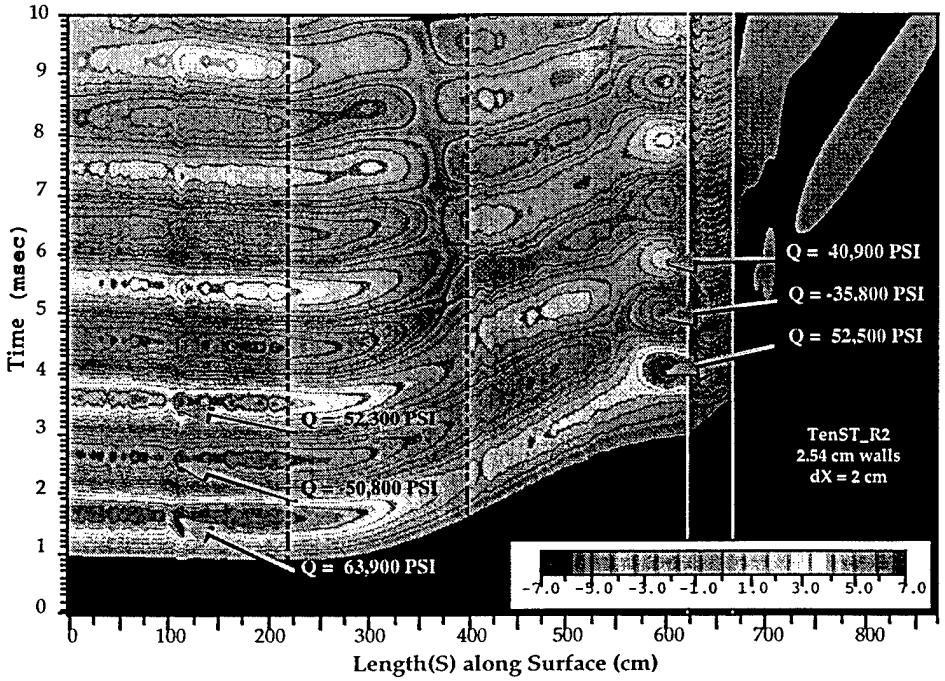

Fig. 10: Tension in the wall as a function of time and wall location for Run 2.

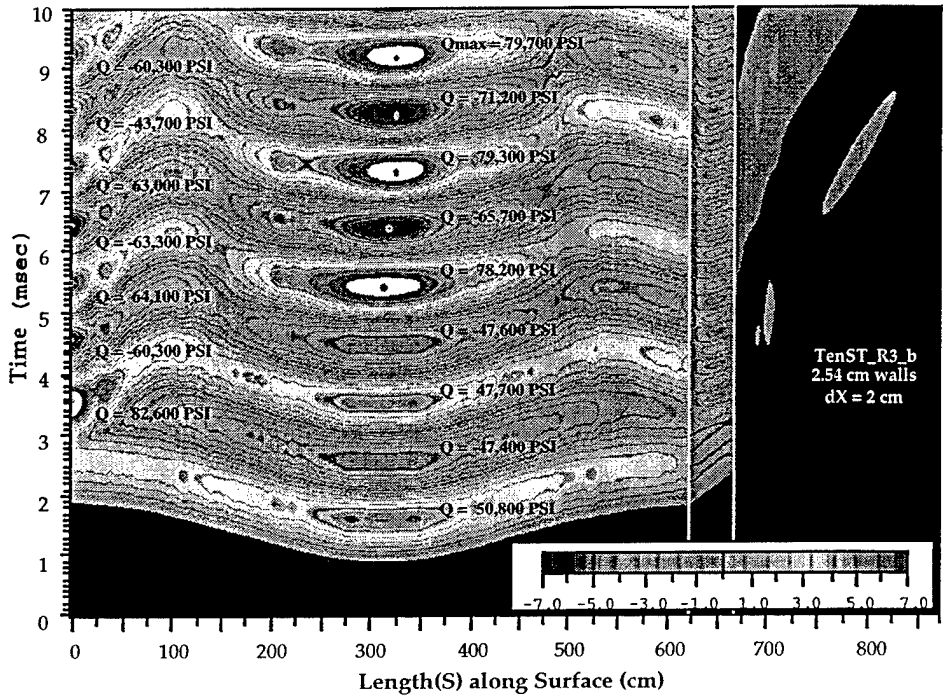

Fig. 11: Tension in the wall as a function of time and wall location for Run 3.

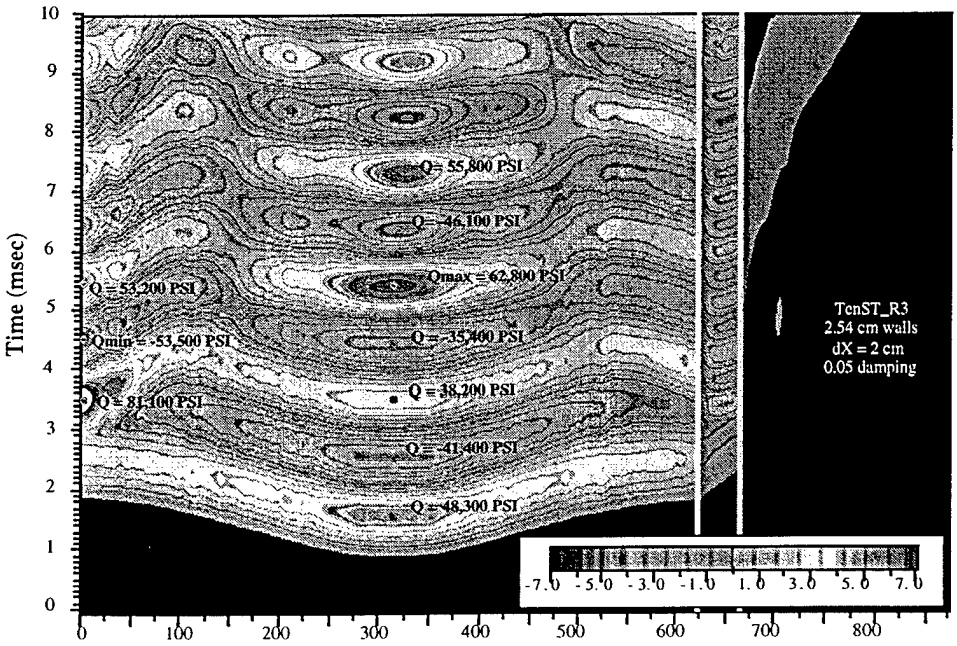

Fig. 12: Tension in the wall as a function of time and wall location for Run 3 with 5% damping.

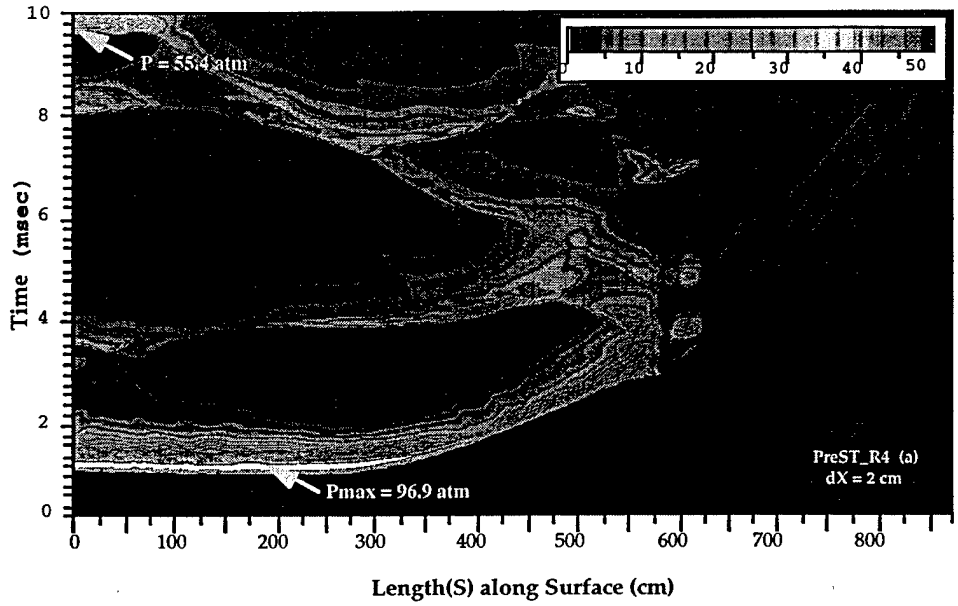

Fig. 13: Pressure as a function of time (0 - 10 ms) and wall location for Run 4. (2.54 cm. walls, 2 cm. grid spacing, 1.82 m. height of detonation, 50 lbs. RDX and 1.5 m opening.)

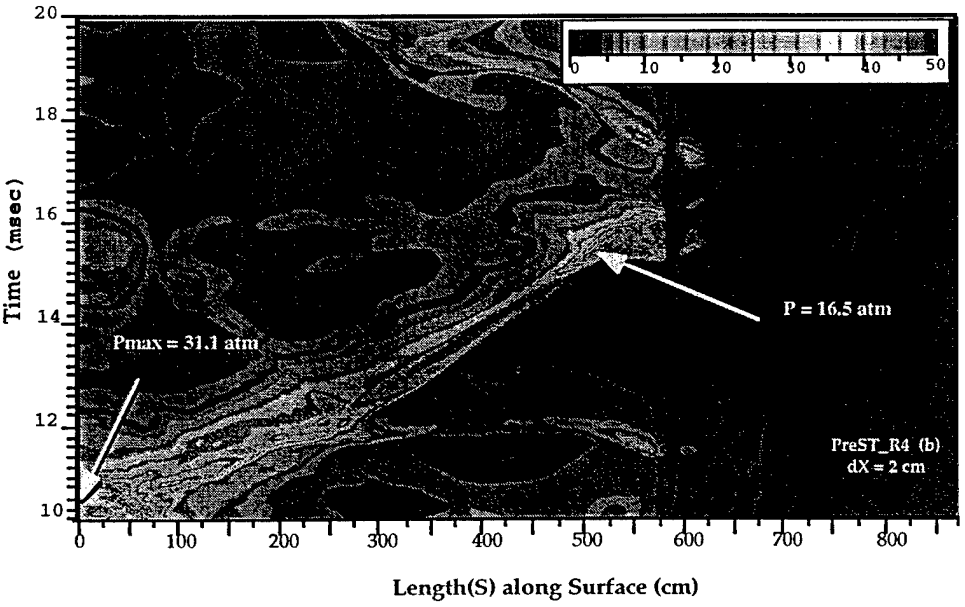

Fig. 14: Pressure as a function of time (15 - 20 ms) and wall location for Run 4.

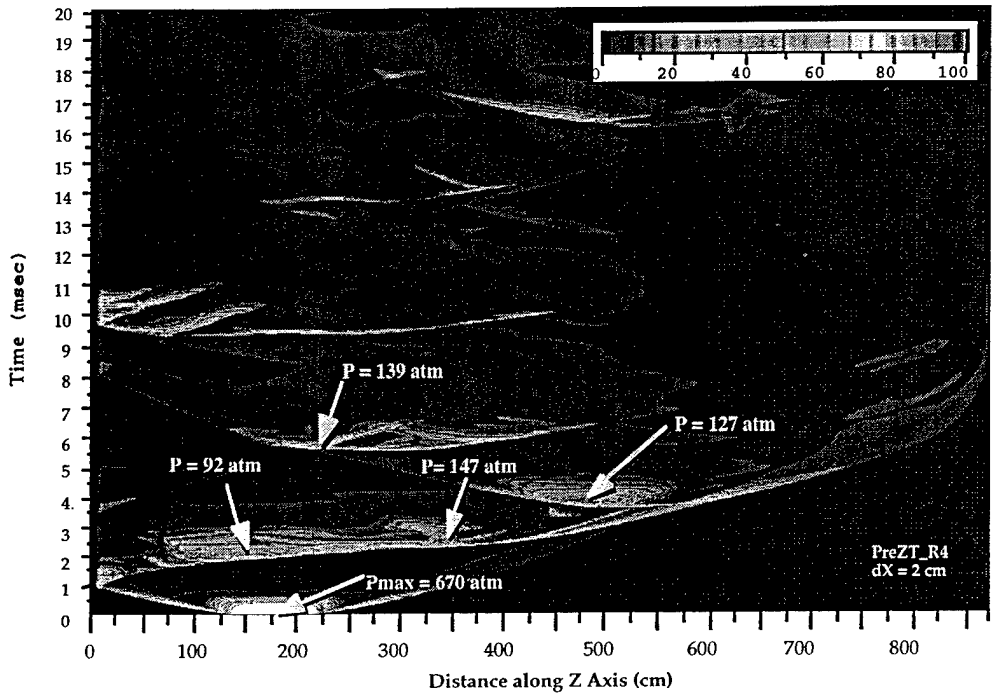

Fig. 15: Pressure as a function of time and centerline location for Run 4.

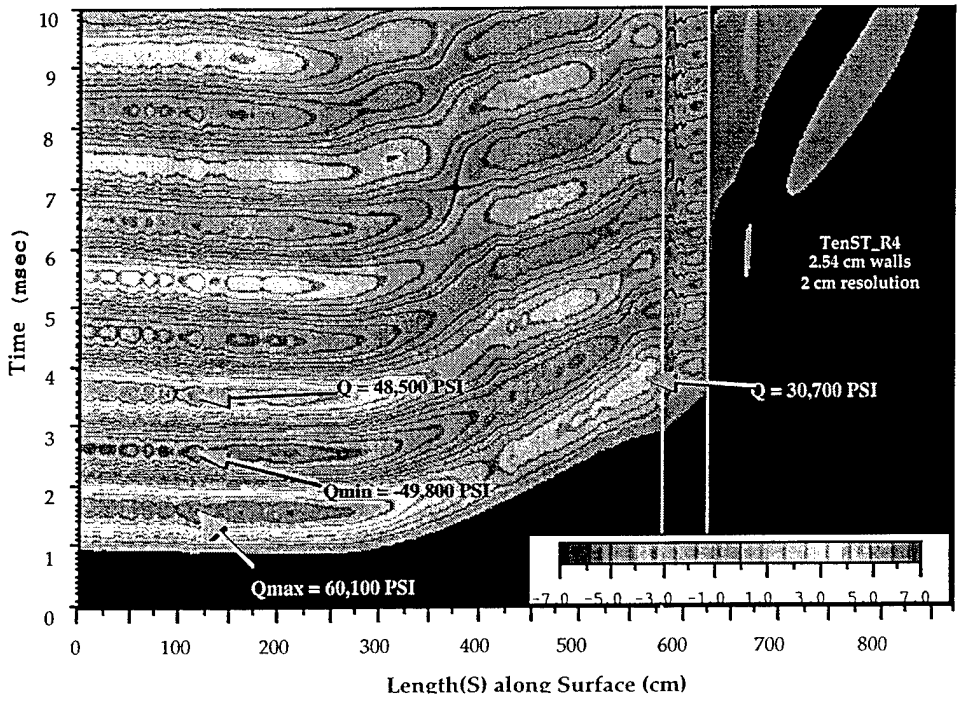

Fig. 16: Tension in the wall as a function of time and wall location for Run 4.

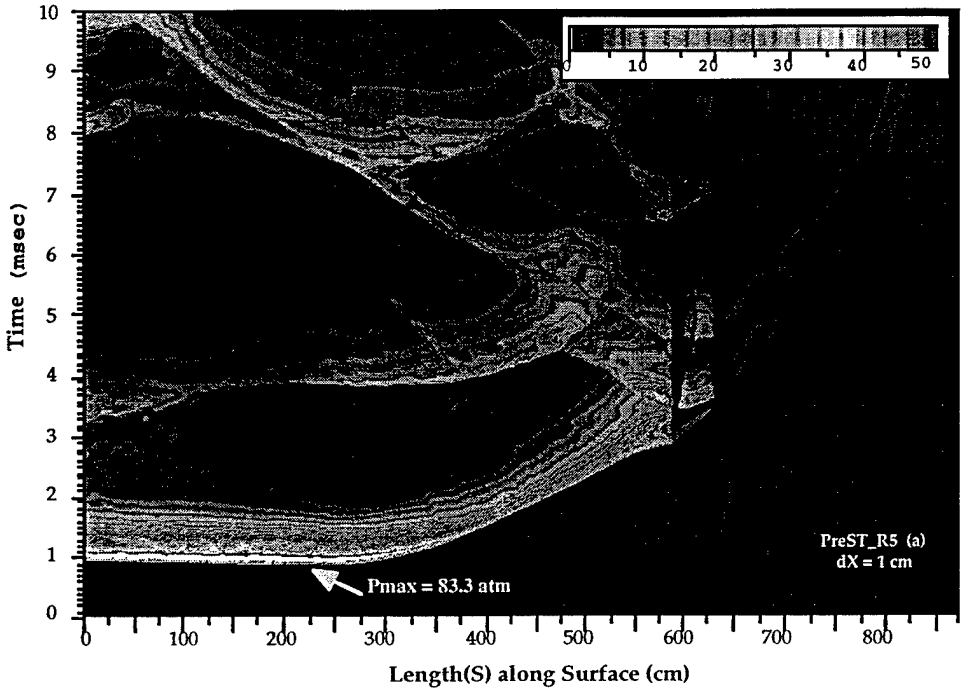

Fig. 17: Pressure as a function of time and wall location for Run 5. (2.54 cm. walls, 1 cm. grid spacing, 1.82 m. height of detonation, 50 lbs. RDX and 1.5 m opening.)

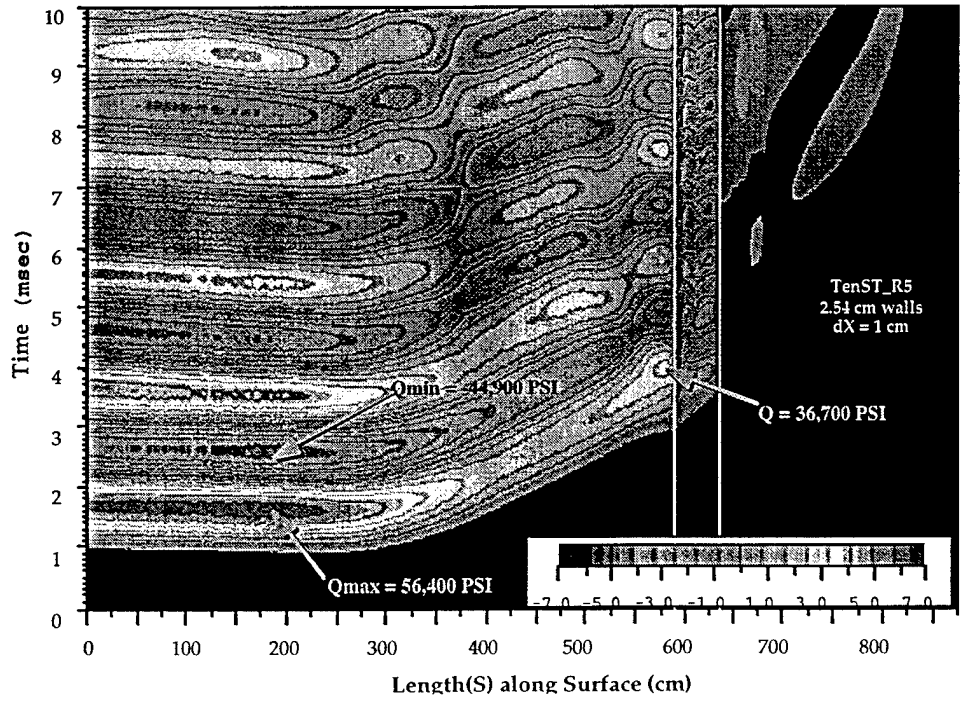

Fig. 18: Tension in the wall as a function of time and wall location for Run 5.

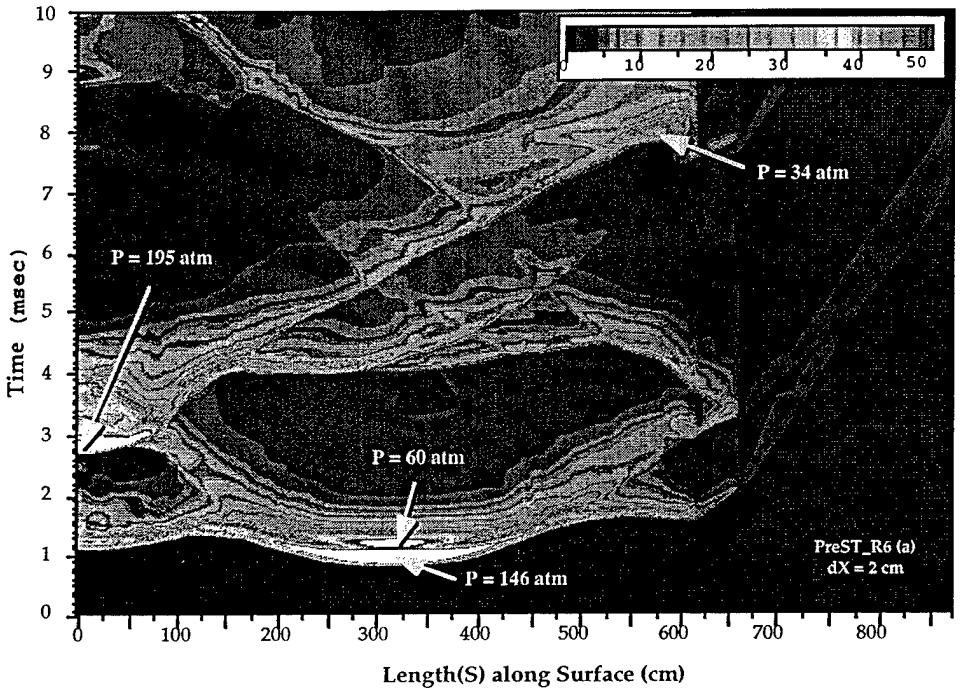

Fig. 19: Pressure as a function of time and wall location for Run 6. (2.54 cm. walls, 2 cm. grid spacing, 1.82 m. height of detonation, 50 lbs. cylindrically shaped RDX and, 1.5 m opening.)

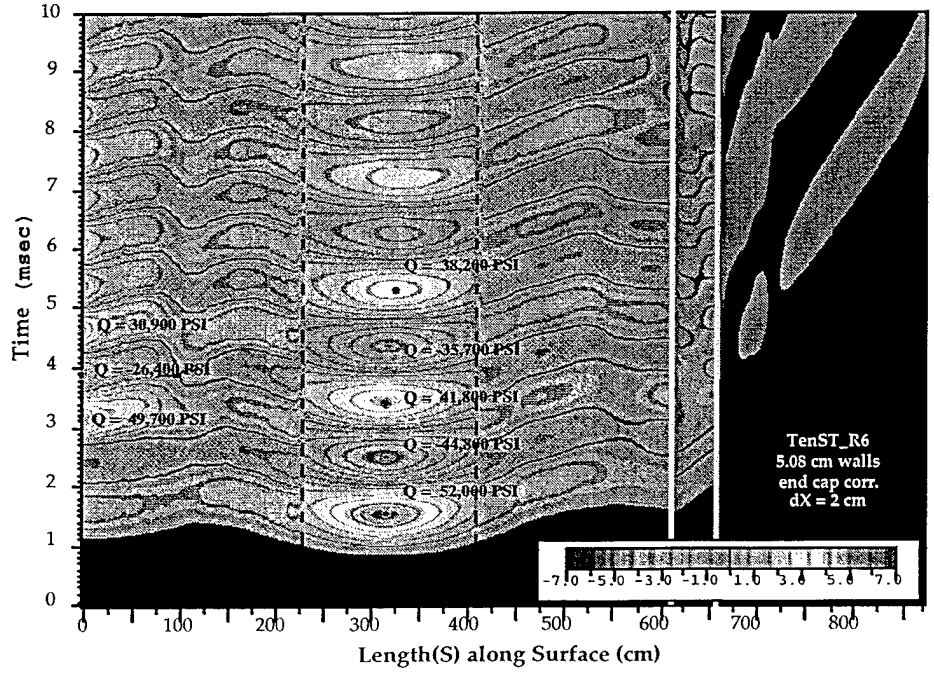

Fig. 20: Tension for the 50 lb cylindrical charge with 5% damping and end cap correction.

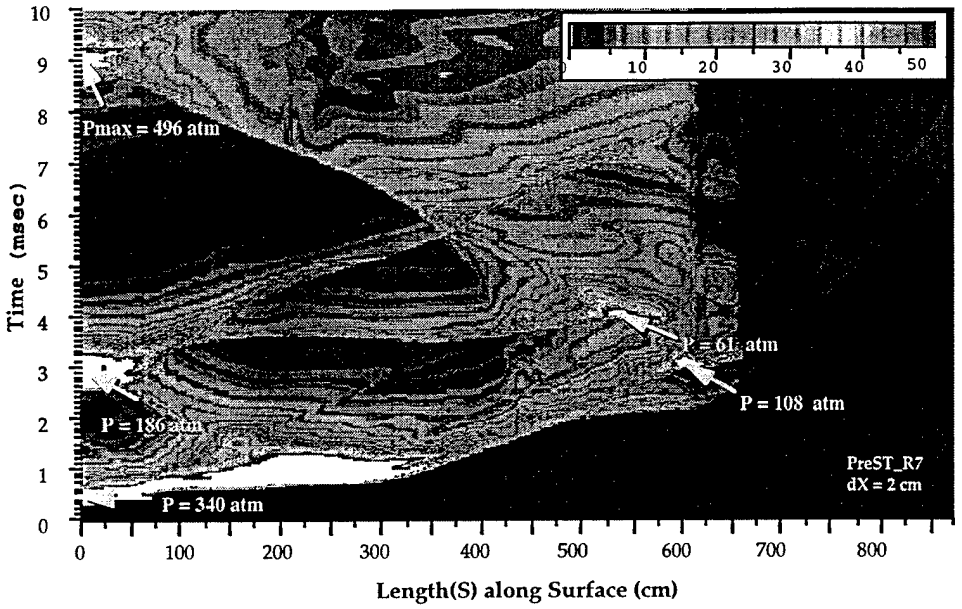

Fig. 21: Pressure as a function of time and wall location for Run 7. (2.54 cm. walls, 2 cm. grid spacing, 1.82 m. height of detonation, 100 lbs. cylindrically shaped RDX and, 1.5 m opening.)

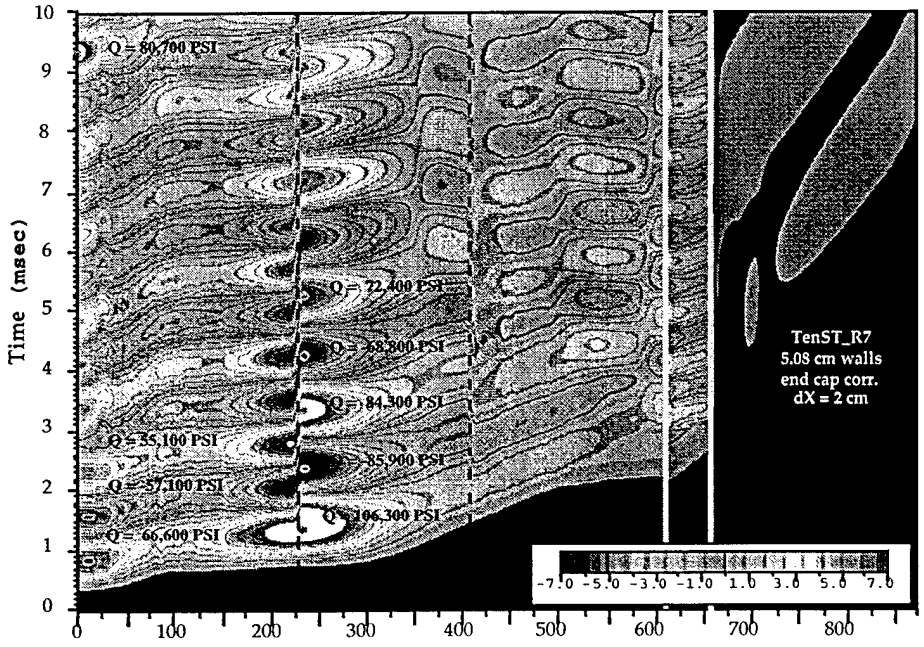

Fig. 22: Tension in the wall as a function of time and wall location for Run R7 with 5% damping and end cap correction.